Surface-induced multiple reentrant transitions

B. K. McCoy,[1] Z. Q. Liu,[1] S. T. Wang,[1] V. P. Panov,[2] J. K. Vij,[2] J. W. Goodby,[3] and C. C. Huang[1]
[1]*School of Physics and Astronomy, University of Minnesota, Minneapolis, Minnesota 55455, USA*
[2]*Department of Electronic and Electrical Engineering, Trinity College, Dublin 2, Ireland*
[3]*Department of Chemistry, University of York, York, YO10 5DD, United Kingdom*
(Received 23 November 2005; published 10 April 2006)

We have studied tilted surface layers in the bulk SmA temperature window of one liquid crystal using null transmission ellipsometry. Five distinct nonplanar surface structures were observed. We present analyses of the tilt and azimuthal profiles of the structures and examine the transitions between the structures. The transitions are identified as a double reentrant synclinic-anticlinic-synclinic-anticlinic transition. Meanwhile, the transitions also display reentrant ferroelectric-antiferroelectric-ferroelectric behavior.

DOI: 10.1103/PhysRevE.73.041704 PACS number(s): 61.30.Hn, 64.70.Md, 77.84.Nh

I. INTRODUCTION

Bulk liquid crystals (LCs) exhibit a rich array of phases depending on temperature, e.g., isotropic liquid, nematic, smectic A (SmA), and a variety of smectic C* (SmC*) variant phases. The smectic phases form a layered structure, which allows for stable free-standing films to be prepared using many compounds. In the SmA phase, the molecular long axis, described by the director **n**, is parallel to the layer normal. In the SmC* variant phases, the molecules are tilted at an angle θ with respect to the normal. In this case, the *c* director, defined by the projection of **n** in the layer plane, is useful for discussing molecular orientations. Many experiments have observed the existence of tilted surface layers at temperatures well above the bulk SmA $\rightarrow$ SmC* transition temperature. For many LC compounds, surfaces tend to be more ordered than the bulk sample, in stark contrast to typical crystalline solids. This phenomenon, known as surface freezing, has been explained in terms of suppression of fluctuations at the surface due to surface tension [1]. Layers containing tilted molecules are optically biaxial. Thus, films consisting of bulk SmA with SmC* surfaces are biaxial only at the surface. This allows for easy measurement of the surface properties with very little interference from the bulk using proper optical probes.

The structures of surface layers above the bulk SmA-SmC* transition have attracted much interest in recent years. Each surface may contain several layers of tilted molecules. θ decreases exponentially with distance away from the surface of the film; typical coherence lengths are on the order of a few smectic layers. Most previous experimental results are explained in terms of an Ising-like model, with coplanar *c* directors for all tilted layers. The molecular orientation may be either symmetric (anticlinic) or antisymmetric (synclinic) about the center of the film. One experiment observed nonplanar tilts [2]. Both synclinic [3,4] and anticlinic [4,5] structures have been observed when no electric field is present. By applying an electric field, transitions from synclinic to anticlinic structures [4,6] and from anticlinic to synclinic structures [4,7] have been observed. Transitions may also occur upon changing the temperature of a film. In two remarkable cases, a reentrant synclinic-anticlinic-synclinic transition [8] and a double reentrant synclinic-anticlinic-synclinic-anticlinic transition [9] were observed. Various models to explain the stability of the synclinic and anticlinic structures have included elastic energy due to spatial variations of **n**, coupling between the applied electric field and the polarization induced by the tilt [10], and polarization fluctuations at the two surfaces [4]. Synclinic structures have polarization perpendicular to the tilt plane and anticlinic structures have polarization parallel to the tilt plane.

If chiral compounds showing the antiferroelectric (SmC$^*_A$) phase are used, interactions beyond nearest neighbor layers give rise to new bulk structures like the SmC$^*_\alpha$, SmC$^*_{FI1}$, and SmC$^*_{FI2}$ phases [11–19]; these structures are not Ising-like. In SmC$^*_\alpha$, the *c* directors rotate by a constant angle between any two adjacent layers, creating an incommensurate helical superstructure. SmC$^*_{FI1}$ (SmC$^*_{FI2}$) is best described by a three (four) layer structure in the distorted clock model [20]. The presence of these more complicated phases in the bulk sample suggests that surface structures may be more complex than Ising-like models under appropriate conditions. Reference [21] reported antiferroelectric coupling between adjacent surface layers, similar to the bulk SmC$^*_A$ phase. The chiral compound (S)12OF1M7 was studied in this experiment. The molecular structure is given in Fig. 1. The bulk phase sequence for (S)12OF1M7 is SmC$^*_A$ (78.4 °C) SmC$^*_{FI1}$ (81.1 °C) SmC$^*_{FI2}$ (84 °C) SmC* (91.3 °C) SmC$^*_\alpha$ (92.4 °C) SmA. A rich sequence of surface transitions in the bulk SmA temperature window was obtained. We will discuss the observed surface structures and analyze the surface transitions. We observed a double reentrant synclinic-anticlinic-synclinic-anticlinic transition and a simultaneous reentrant ferroelectric-antiferroelectric-ferroelectric transition.

II. EXPERIMENTAL SETUP

Null transmission ellipsometry (NTE) is a technique particularly well-suited for studying optical properties of thin

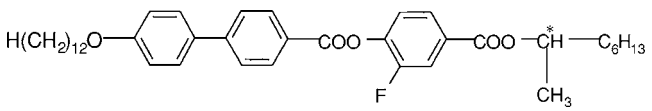

FIG. 1. Chemical structure of (S)12OF1M7.

 ©2006 The American Physical Society

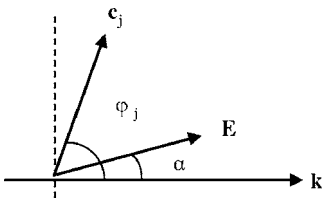

FIG. 2. Definition of angles used in the text. **k** is the projection of the wave vector of the incident light on the film plane. **E** is the direction of the applied electric field. $\mathbf{c}_j$ is the c director of the jth layer.

surface layers. Elliptically polarized laser light is transmitted through a free-standing film with anisotropic optical properties. The sample introduces a phase lag between the $\hat{p}$ and $\hat{s}$ components of the polarization, causing a change in the ellipticity of the polarization state of the laser light. The phases of the components of the incident light are adjusted so that the transmitted light is linearly polarized. Two ellipsometric parameters are measured: Ψ and Δ. Ψ measures the phase difference between the incident $\hat{p}$ and $\hat{s}$ components necessary to produce linearly polarized light and Δ is the polarization angle of the transmitted light. A detailed description of our NTE apparatus can be found in Ref. [22].

Inside a temperature-regulated two-stage oven, thin free-standing liquid crystal films are created by pulling the sample across a hole of radius 7 mm in a glass coverslip. The free-standing film geometry ensures that the smectic layers are parallel to the film plate. An electric field is applied using eight electrodes placed symmetrically about the hole in the coverslip. The electric field is in the plane of the film and uniform except for very near the electrodes. The spontaneous polarization of the film aligns with the electric field, producing a stable monodomain sample. The electric field is small enough that the film structure is not altered by the field. By varying the voltages on the electrodes, the electric field and molecular orientations can be controlled. In this paper, the orientation of the electric field will be denoted by α, the angle between the electric field and the incident plane (see Fig. 2).

III. EXPERIMENTAL DATA

The parameters Ψ and Δ were measured for several 16-layer films as the temperature was ramped at a rate of 20 mK/min. Here we will only discuss Δ; one can see in Fig. 3 that Ψ shows similar features. Both heating and cooling ramps were performed to check for reproducibility. The electric field orientation was switched between 0° and 90° every 2.5 min during the temperature ramps. Figure 3 shows Δ as a function of temperature for both orientations (Δ_0 and Δ_{90}). Five distinct surface structures are evident. Above T_5 the bulk is uniaxial SmA, so the features of the curves in Fig. 3 are dominated by the biaxiality of the surface layers. Above T_1, Δ is nearly equal at the two orientations, suggesting a synclinic arrangement of the surface layers. As the film is cooled below T_1, a transition in the surface layer structure occurs as evidenced by the jump in Δ_{90}. Upon further cooling, another transition occurs at T_2. The absolute value of

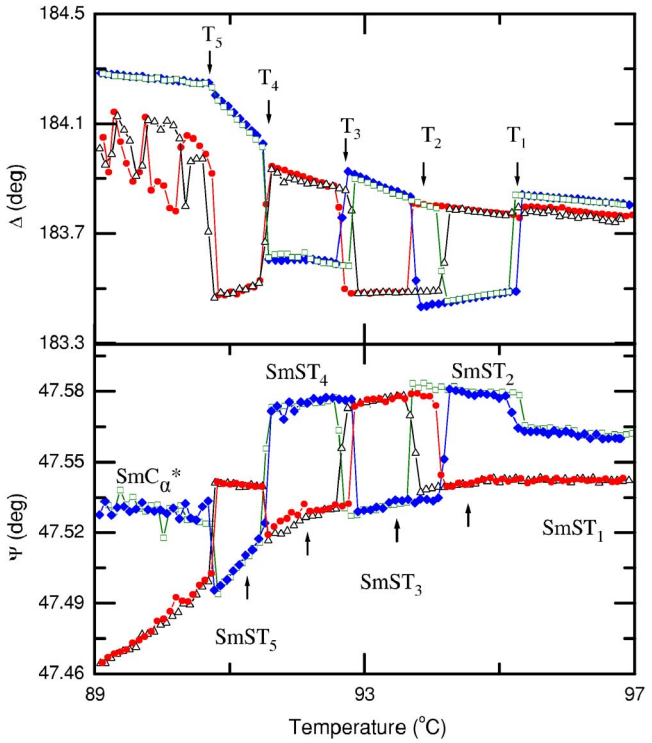

FIG. 3. (Color online) Temperature dependence of Δ and Ψ under two different orientations of E for a 16-layer film. Open (closed) symbols are data obtained while heating (cooling) at a rate of 20 mK/min. The electric field strength was E=7.14 V/cm. Circles and triangles are data obtained at α=0° and squares and diamonds are data obtained at α=90°. Downward arrows mark five transition temperatures. Upward arrows mark the temperatures at which the rotation data in Figs. 4–8 were obtained.

$\Delta_0-\Delta_{90}$ remains nearly constant at T_2. The sign of $\Delta_0-\Delta_{90}$ changes at T_2, suggesting that the molecules rotate about the layer normal by 90° at the transition. Changes in the sign of $\Delta_0-\Delta_{90}$ are also evident at T_3 and T_4. Changes in the magnitude of $\Delta_0-\Delta_{90}$ show that the net biaxiality of the surface layers also changes at T_2, T_3, and T_4, illustrating a more subtle change in the structure than simple rotation of all molecules about the layer normal by 90°. The 90° rotations indicate a change in polarization of the film from longitudinal to transverse, as described in Ref. [10].

We can obtain more detail about the surface layer structure by rotating the direction of the electric field. The ellipsometric parameters were measured as a function of α, with the temperature held constant. A typical data set included rotation of α from 0° to 360° in steps of 10° with several independent measurements of Ψ and Δ at each step to monitor data quality. In order to characterize the surface structures, many rotations were performed at various temperatures. Typical rotation data are given in Figs. 4–8 for one temperature (marked by upward arrow in Fig. 3) in each of the five temperature regions (henceforth labeled $SmST_1$ through $SmST_5$, to denote smectic-surface tilt phases). The differences in these figures confirm that the surface structures change. Figure 4(a) shows rotation data for $SmST_1$. The Δ versus α curve has a pronounced minimum at α=270°. This is a signature of a synclinic surface structure. Figure 5(a)

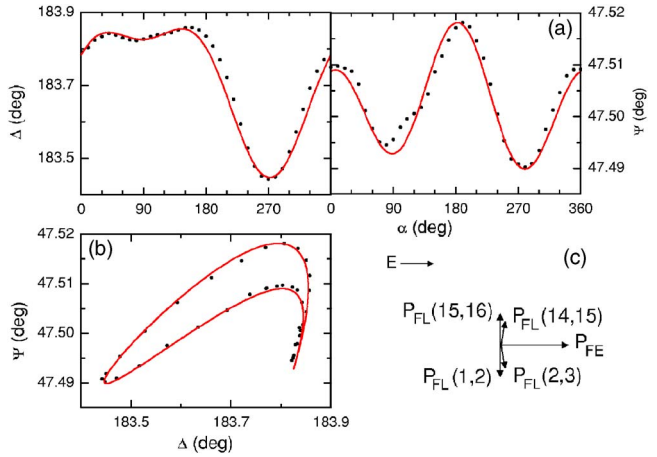

FIG. 4. (Color online) (a) shows dependence of Δ and Ψ on α at $T=102.60$ °C ($SmST_1$). (b) plots Ψ versus Δ. Circles are data and solid lines are simulation results. (c) Shows directions of the components of the polarization for the structure in equilibrium at $\alpha=0°$. The arrows for P_{FE} and P_{FL} are drawn using $e_1=e_2$. The same symbols and scales are used in Figs. 5–8, except where noted. The electric field strength for Figs. 4–8 was $E=7.14$ V/cm.

shows rotation data for $SmST_2$. Both Ψ and Δ are nearly symmetric in a 180° rotation, which could indicate either anticlinic surface layers, or antiferroelectric ordering within each surface. $SmST_3$ [Fig. 6(a)] again shows 180° symmetry, but the maxima and minima are displaced by 90° from Fig. 5(a). This illustrates the 90° rotation of the film that was evident in Fig. 3. Figures 7(a) and 8(a) show the rotation data for $SmST_4$ and $SmST_5$.

IV. DATA ANALYSES

A more detailed analysis using Berreman's 4×4 matrix method [23] is necessary to determine the surface structures.

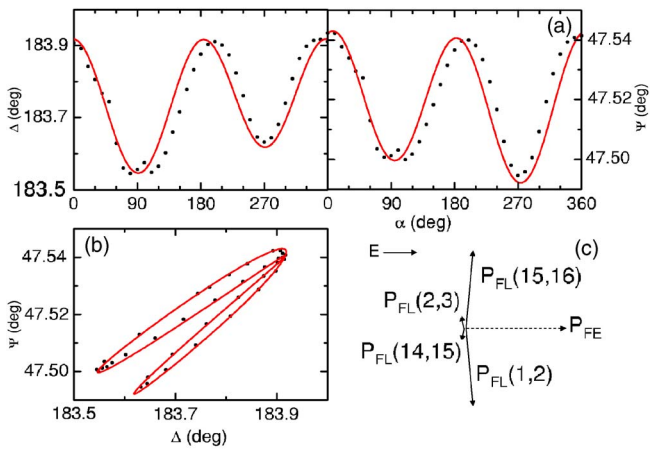

FIG. 5. (Color online) (a) Δ and Ψ versus α and (b) Ψ versus Δ at $T=94.42$ °C ($SmST_2$). (c) Shows directions of the components of the polarization. P_{FE} is very small for this structure because the surfaces are nearly antiferroelectric, so a different scale has been used for the diagram. e_2 is the same for all diagrams, but $e_1=100e_2$ in this figure, in contrast to Figs. 4 and 6–8.

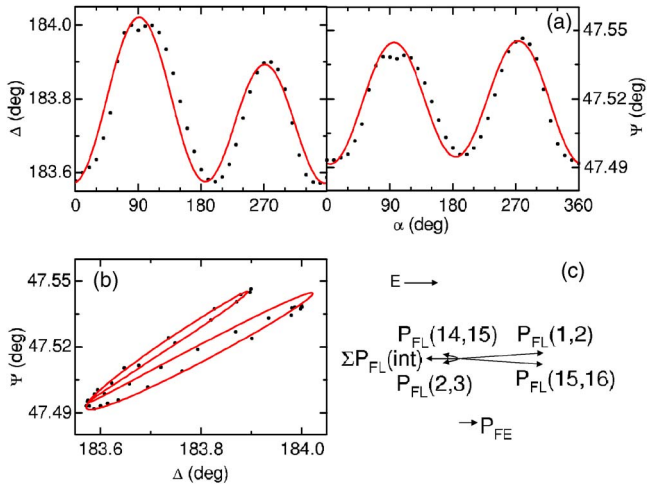

FIG. 6. (Color online) (a) Δ and Ψ versus α and (b) Ψ versus Δ at $T=93.48$ °C ($SmST_3$). (c) Shows directions of the components of the polarization. ΣP_{FL}(int) represents the net P_{FL} from the interior layers.

Berreman's method models each smectic layer as a uniaxial slab with indices of refraction n_e along the long axis of the molecules and n_o perpendicular to the long molecular axis. Maxwell's equations are applied to each layer using an incident electromagnetic (EM) wave and appropriate boundary conditions to get the ellipsometric parameters for the transmitted light beam. n_o and n_e were obtained by spreading 71 films with different thicknesses at 103 °C, in the uniaxial SmA phase. A plot of Ψ versus Δ for these films was compared to simulation using a uniaxial slab with n_o and n_e as free parameters [24]. In SmA, the indices of refraction for this compound are found to be $n_o=1.496\pm0.003$ and $n_e=1.658\pm0.003$. Quantizing the film thickness in the simulation gave a measure of the smectic layer spacing: $d=3.66\pm0.05$ nm. This method also allows measurement of the thickness of films in number of layers. Simulations using the 4×4 matrix method are included in Figs. 4–8.

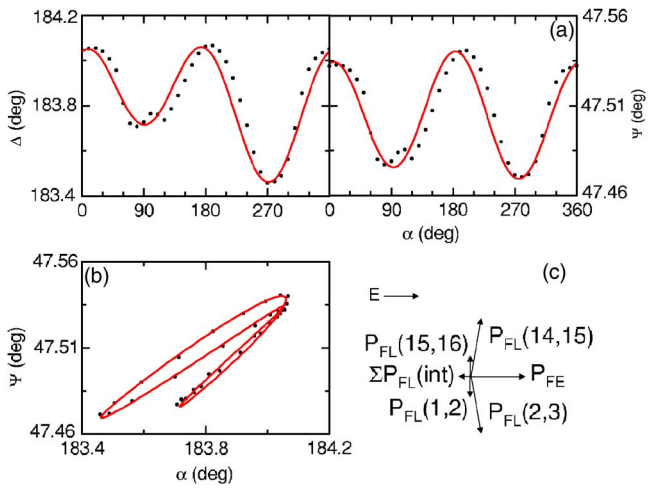

FIG. 7. (Color online) (a) Δ and Ψ versus α and (b) Ψ versus Δ at $T=92.14$ °C ($SmST_4$). (c) Shows directions of the components of the polarization.

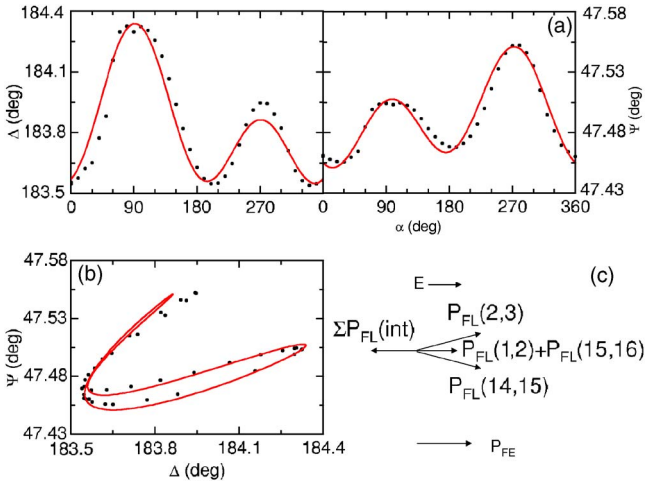

FIG. 8. (Color online) (a) Δ and Ψ versus α and (b) Ψ versus Δ at $T=91.23$ °C ($SmST_5$). (c) Shows directions of the components of the polarization.

Experiments using differential optical reflectivity [25] indicate that in SmC^*_α not more than six surface layers are present in (S)12OF1M7, therefore three tilted layers for each surface were considered. θ_j and φ_j are the tilt and azimuthal angles for the jth layer when $\alpha=0°$ (electric field in the incident plane), as defined in Fig. 2. $j=1$ denotes the first layer on the side of the film from which the laser light is incident. The 32 angles θ_j and φ_j for $j=1-16$ were varied to determine the surface layer structure. The tilt profile was calculated from the mean-field theory result [26]

$$\theta_j = \theta_{\text{surf}} \frac{\cosh\left(\left[2\left(j-\frac{1}{2}\right)-N\right]/2\xi\right)}{\cosh([N-1]/2\xi)}. \tag{1}$$

Here N and ξ are the film thickness and correlation length in number of smectic layers. Because the inner layers have small tilt angles, the simulations are not sensitive to their azimuthal orientations, so for convenience we assumed $\varphi_j=\varphi_3$ for $j=4-8$ and $\varphi_j=\varphi_{14}$ for $j=9-13$. φ_1 and φ_{16} were determined by the symmetry of the Ψ and Δ versus α curves. Symmetry about the vertical center of the film further constrains the azimuthal orientations for the surface layers, so that only the parameters φ_2 and φ_3 needed to be varied to determine each structure, along with increases of θ_{surf} and ξ with decreasing temperature.

Before discussing the structures, some comments on polarization in chiral smectic LCs are necessary. Two types of polarization are possible due to molecular orientations in smectic layers: ferroelectric polarization (P_{FE}) and flexoelectric polarization (P_{FL}). The ferroelectric polarization density in each layer is a result of chiral symmetry breaking when molecules are tilted. P_{FE} is perpendicular to the c director for each layer and approximately proportional to the tilt angle

$$\vec{P}_{\text{FE}} \approx e_1\theta(\sin\varphi, -\cos\varphi, 0). \tag{2}$$

P_{FL} results from gradients of $\mathbf{n}$. In a continuum description, the flexoelectric polarization density is given by

$$\vec{P}_{\text{FL}} = e_2\mathbf{n}\times(\boldsymbol{\nabla}\times\mathbf{n}), \tag{3}$$

where e_2 is a flexoelectric coefficient [27]. Other flexoelectric terms have been neglected because they yield qualitatively similar results. For smectic LCs, Eq. (2) can be discretized to find the flexoelectric polarization between two adjacent layers. The direction of P_{FL} is easily calculated from the tilt and azimuthal angle of adjacent layers.

$$\vec{P}_{\text{FL}}(j,j+1) = \frac{e_2}{2}(\mathbf{n_j}+\mathbf{n_{j+1}})\times(-\mathbf{n_{j,y}}+\mathbf{n_{j+1,y}}, \mathbf{n_{j,x}}-\mathbf{n_{j+1,x}}, \mathbf{0}). \tag{4}$$

In bulk samples, net P_{FL} vanishes, but in thin films, P_{FL} may be comparable to P_{FE} [10].

The parameters for the best fits to all data shown in Figs. 4–8 are listed in Table I along with estimated uncertainties. The uncertainty given for each parameter was chosen by holding the other parameters constant while varying the parameter in question to determine the range of acceptable values. In addition to the experimental data and fitting curves, Figs. 4–8 also give the directions of various polarization contributions. Currently we do not have a good estimate of their magnitudes. First, within $SmST_1$ (see Fig. 4), the structure consists primarily of two layers at each surface. The coupling between the first and second layers is ferroelectric

TABLE I. This table summarizes the parameters for the best fits to Figs. 4–8.

	$SmST_1$	$SmST_2$	$SmST_3$	$SmST_4$	$SmST_5$
θ_{surf} (deg)	18.4±0.2	25.3±0.3	26.5±0.4	27.3±0.3	29.5±0.5
ξ (layers)	0.95±0.05	1.45±0.02	1.60±0.05	1.96±0.05	2.31±0.1
φ_1 (deg)	270±1	270±2.5	0±2.5	270±3	0±5
φ_2 (deg)	270±7	102±3	193±3	270±5	0±10
φ_3 (deg)	120±15	102±7	193±5	103±6	216±5
φ_{14} (deg)	60±15	78±7	347±5	77±6	324±5
φ_{15} (deg)	270±7	78±3	347±3	270±5	180±10
φ_{16} (deg)	270±1	270±2.5	180±2.5	270±3	180±5

and the two surfaces are in a synclinic arrangement. Here we use ferroelectric (antiferroelectric) to mean that the c directors for the first and second layers are parallel (antiparallel) and synclinic (anticlinic) to mean that the c directors for the first and 16th layers are parallel (antiparallel). θ_{surf} and ξ are determined by the amplitudes of the Ψ and Δ versus α curves. The tilts for the third and 14th layers must be nonplanar in order to produce the sizable difference between Ψ_{90} and Ψ_{270}. $\Psi_{90}-\Psi_{270}>0$ requires that φ_3 be in the second quadrant; by symmetry, φ_{14} is in the 1st quadrant. The shape of the Ψ versus Δ curve determines the magnitude of the nonplanar angle. Fits at different temperatures in $SmST_1$ indicate that the nonplanar angle varies with temperature. For example, just above T_1, φ_{14} is in the fourth quadrant and φ_3 is in the third quadrant. Figure 4(c) shows a polarization diagram for the structure at $T=102.60$ °C. Net P_{FE} and P_{FL} are both perpendicular to the tilt plane of the outermost layers, in the direction of the electric field.

Both θ_{surf} and ξ in $SmST_2$ increased from those found in $SmST_1$. The shape of the Ψ versus Δ curve places a tight constraint on the value of ξ. The two outermost surfaces are still in a synclinic arrangement, but the coupling between the first and second layers is now nearly antiferroelectric. The opening of the two leaves of the Ψ versus Δ curve depends on the nonplanar angle. If the assumption that $\varphi_2=\varphi_3$ is relaxed, satisfactory fits can also be obtained provided that the sum of the c directors for $j=2-15$ remains the same. Because the surfaces are nearly antiferroelectric, the net P_{FE} nearly cancels. P_{FE} is small and parallel to the electric field. The net P_{FL} is larger than for the structure in $SmST_1$ and antiparallel to the electric field [see Fig. 5(c)]. This implies that P_{FE} is still the dominant contribution to the net polarization of the film.

The tilt plane of the outermost layers in $SmST_3$ is perpendicular to that in $SmST_2$. The outermost layers are anticlinic. The angles between the c directors for the first and second layers and the 15th and 16th layers are nearly equal to the previous structure. This structure can be obtained by rotating the surface on the incident side of the film clockwise by 90° and rotating the opposite surface counterclockwise by 90°. The net P_{FE} has magnitude larger than P_{FE} for $SmST_2$, but smaller than P_{FE} for $SmST_1$. The net P_{FE} for $SmST_3$ is in the direction of the electric field. The dominant contributions to P_{FL} are nearly aligned for this structure, so there is a large net P_{FL} in the direction of the electric field. See Fig. 6.

Our simulation results from the data in $SmST_4$ show that the coupling between the first and second layers is ferroelectric and that the two surfaces are synclinic. The Ψ versus Δ and Ψ versus α curves are similar to those for $SmST_2$, while the Δ versus α curve is shifted by 180°. The structure for $SmST_2$ cannot produce this different behavior in Δ versus α for any value of the angle between the c directors for the first and second layers. The data for $SmST_1$ shows similar features in both the Ψ and Δ versus α curves. The minimum at $\alpha=90°$ in the Δ versus α curve for $SmST_1$ is a result of the nonplanar tilt of the third layer. As the tilt of the third layer increases, the minimum in the Δ versus α curve at $\alpha=90°$ becomes more pronounced. Simulations using a structure qualitatively identical to the structure for $SmST_1$ fit the data quite well when θ_{surf} and ξ are increased to account for the decrease in temperature and φ_3 is adjusted to fit the maxima and minima of the Ψ and Δ versus α curves. The net P_{FE} is in the direction of the electric field. P_{FL} is small for this structure and dominated by the interior layers. The net P_{FL} is antiparallel to the electric field.

In $SmST_5$, the coupling between the first and second layers is ferroelectric, but the two surfaces are in an anticlinic arrangement. This structure can be obtained by rotating the two surfaces in opposite directions as described previously for the $SmST_2 \rightarrow SmST_3$ transition. This fit is less satisfactory than the fits for $SmST_1$-$SmST_4$. With increasing ξ, the interior layers play a larger role and the assumption that $\varphi_j=\varphi_3$ for $j=4-8$ and $\varphi_j=\varphi_{14}$ for $j=9-13$ may no longer be appropriate. The net P_{FE} for this structure is in the tilt plane of the outermost layers, parallel to the electric field. The net P_{FL} for this structure is relatively large and also in the direction of the electric field.

V. DISCUSSION

Two distinct types of reentrant behavior are evident in these data. The molecular arrangements in the outermost two layers in $SmST_1$, $SmST_2$, and $SmST_4$ are synclinic, while those in $SmST_3$ and $SmST_5$ are anticlinic. There is a double reentrant synclinic-anticlinic-synclinic-anticlinic transition similar to the transition observed in Ref. [9]. Under some circumstances single reentrant behavior may be explained by the coupling between the electric field and P_{FE}, while ignoring P_{FL} [5], by using a phenomenological model to calculate the elastic energies of the synclinic and anticlinic structures when no applied field is present. In Ref. [5], a term is added to the free energy of the synclinic state to account for the coupling of P_{FE} to the electric field. Adding a free energy term that couples P_{FL} to the electric field in a similar manner can in principle account for a double reentrant transition. This model requires an electric field to produce the reentrant transition and the transition temperatures are dependent on the magnitude of the electric field. We have performed temperature ramps similar to Fig. 3 with two different electric field strengths: $E=0.143$ V/cm and $E=14.3$ V/cm. Measurements with $E=0$ V/cm are not feasible because we require an electric field to orient the molecules. All five surface structures appeared for each electric field strength and the transition temperatures were equal within our resolution. This implies that the transitions are not driven by the electric field. The anticlinic and synclinic structures are stabilized by some long-range interaction that is not well understood. Both the $SmST_2 \rightarrow SmST_3$ and $SmST_4 \rightarrow SmST_5$ transitions show dramatic increases in the net P_{FL}, while the coupling between adjacent layers remains the same. This suggests that P_{FL} plays some role in the transitions.

Each of the structures observed contains nonplanar tilts within each surface, in contrast to the Ising-like models considered in previous experiments. Nonplanar tilts are present in bulk samples in the SmC^*_α, SmC^*_{FI1}, and SmC^*_{FI2} phases. The structures $SmST_{1-5}$ can be viewed as precursors of these bulk SmC^* variant phases. The SmC^* variant phases are predicted by a phenomenological model including third nearest neighbor coupling terms, in which interlayer interactions

vary with temperature [11,12]. Nonplanar structures occur when nearest neighbor (nn) interactions are ferroelectric and next nearest neighbor (nnn) interactions are antiferroelectric. In $SmST_1$, the first and second *c* directors are nearly parallel so the nn interaction dominates. In $SmST_2$ and $SmST_3$, the first and second *c* directors are nearly antiparallel and the second and third *c* directors are parallel. The nonplanar angles in $SmST_2$ and $SmST_3$ are small, so these structures can be viewed as precursors of the bulk antiferroelectric or ferrielectric phases. In $SmST_4$ and $SmST_5$, the first and second *c* directors are parallel and the third *c* director is nearly antiparallel. nn interactions dominate at the surface and nnn interactions play a larger role further away from the surface. The structures exhibited in this compound are rather complicated, making it difficult to glean concrete information about the relative strengths of the nn and nnn interactions. Compounds with surface structures intermediate in complexity between (S)12OF1M7 and the compounds that gave Ising-like structures may be useful for exploring the effects of tilt and temperature on the nn and nnn interactions. The second type of reentrant transition alluded to earlier is evident in the relative orientations of the molecules in the first and second layers. There is a ferroelectric-antiferroelectric-ferroelectric transition. To the best of our knowledge, no other LC systems exhibit ferroelectric-antiferroelectric-ferroelectric transitions and such transitions are rare in other systems as well. At this time, we have no explanation for this phenomenon.

In conclusion, we have determined the surface structures for a complicated set of surface transitions using NTE. Five nonplanar structures were observed, showing that typical Ising-like models of surface structures are inadequate for this compound. The complicated sequence of transitions is driven simultaneously by long-range and short-range interactions. Current theoretical models cannot explain the double reentrant synclinic-anticlinic-synclinic-anticlinic transition or the reentrant ferroelectric-antiferroelectric-ferroelectric transition.

ACKNOWLEDGMENTS

This research was supported in part by the Donors of the Petroleum Research Fund, administered by the American Chemistry Society, and by the National Science Foundation, Solid State Chemistry Program under Grant No. DMR-0106122. V.P. is supported by the Irish Council for Science and Engineering. Sample preparation was funded by the EU Sampa Project.

[1] R. Hołyst, Phys. Rev. A **44**, 3692 (1991).
[2] X. F. Han, D. A. Olson, A. Cady, D. R. Link, N. A. Clark, and C. C. Huang, Phys. Rev. E **66**, 040701(R) (2002).
[3] Ch. Bahr and D. Fliegner, Phys. Rev. Lett. **70**, 1842 (1993).
[4] P. M. Johnson, D. A. Olson, S. Pankratz, Ch. Bahr, J. W. Goodby, and C. C. Huang, Phys. Rev. E **62**, 8106 (2000).
[5] B. Rovšek, M. Čepič, and B. Žekš, Phys. Rev. E **66**, 051701 (2002).
[6] S. T. Wang, X. F. Han, Z. Q. Liu, A. Cady, M. D. Radcliffe, and C. C. Huang, Phys. Rev. E **68**, 060702(R) (2003).
[7] D. R. Link, G. Natale, N. A. Clark, J. E. Maclennan, M. Walsh, S. S. Keast, and M. E. Neubert, Phys. Rev. Lett. **82**, 2508 (1999).
[8] C. Y. Chao, C. R. Lo, P. J. Wu, Y. H. Liu, D. R. Link, J. E. Maclennan, N. A. Clark, M. Veum, C. C. Huang, and J. T. Ho, Phys. Rev. Lett. **86**, 4048 (2001).
[9] X. F. Han, S. T. Wang, A. Cady, M. D. Radcliffe, and C. C. Huang, Phys. Rev. Lett. **91**, 045501 (2003).
[10] P. O. Andreeva, V. K. Dolganov, and K. P. Meletov, JETP Lett. **66**, 442 (1997).
[11] E. Gorecka, D. Pociecha, M. Čepič, B. Žekš, and R. Dabrowski, Phys. Rev. E **65**, 061703 (2002).
[12] D. A. Olson, X. F. Han, A. Cady, and C. C. Huang, Phys. Rev. E **66**, 021702 (2002).
[13] M. B. Hamaneh and P. L. Taylor, Phys. Rev. Lett. **93**, 167801 (2004).
[14] M. B. Hamaneh and P. L. Taylor, Phys. Rev. E **72**, 021706 (2005).
[15] P. V. Dolganov, V. M. Zhilin, V. K. Dolganov, and E. I. Kats, Phys. Rev. E **67**, 041716 (2003).
[16] A. V. Emelyanenko and M. A. Osipov, Phys. Rev. E **68**, 051703 (2003).
[17] P. Mach, R. Pindak, A.-M. Levelut, P. Barois, H. T. Nguyen, C. C. Huang, and L. Furenlid, Phys. Rev. Lett. **81**, 1015 (1998).
[18] D. Schlauf, Ch. Bahr, and H. T. Nguyen, Phys. Rev. E **60**, 6816 (1999).
[19] P. M. Johnson, S. Pankratz, P. Mach, H. T. Nguyen, and C. C. Huang, Phys. Rev. Lett. **83**, 4073 (1999).
[20] P. M. Johnson, D. A. Olson, S. Pankratz, T. Nguyen, J. Goodby, M. Hird, and C. C. Huang, Phys. Rev. Lett. **84**, 4870 (2000); A. Cady, J. A. Pitney, R. Pindak, L. S. Matkin, S. J. Watson, H. F. Gleeson, P. Cluzeau, P. Barois, A. M. Levelut, W. Caliebe, J. W. Goodby, M. Hird, and C. C. Huang, Phys. Rev. E **64**, 050702(R) (2001).
[21] X. F. Han, D. A. Olson, A. Cady, J. W. Goodby, and C. C. Huang, Phys. Rev. E **65**, 010704(R) (2001).
[22] D. A. Olson, X. F. Han, P. M. Johnson, A. Cady, and C. C. Huang, Liq. Cryst. **29**, 1521 (2002).
[23] D. W. Berreman, J. Opt. Soc. Am. **62**, 502 (1972); H. Wohler, G. Haas, M. Fritsch, and D. A. Mlynski, J. Opt. Soc. Am. A **5**, 1554 (1988).
[24] C. C. Huang, S. T. Wang, X. F. Han, A. Cady, R. Pindak, W. Caliebe, K. Ema, K. Takekoshi, and H. Yao, Phys. Rev. E **69**, 041702 (2004).
[25] V. P. Panov, B. K. McCoy, Z. Q. Liu, J. K. Vij, J. W. Goodby, and C. C. Huang (unpublished).
[26] C. Bahr, C. J. Booth, D. Fliegner, and J. W. Goodby, Phys. Rev. E **52**, R4612 (1995).
[27] P. G. DeGennes and J. Prost, *The Physics of Liquid Crystals* (Clarendon Press, Oxford, 1993).